Frequency-Modulated Charge Pumping With Extremely High Gate Leakage

Jason Thomas Ryan, *Member, IEEE*, Jibin Zou, *Student Member, IEEE*, Richard Southwick, III, *Member, IEEE*, Jason Paul Campbell, *Member, IEEE*, Kin P. Cheung, *Senior Member, IEEE*, Anthony S. Oates, *Fellow, IEEE*, and Ru Huang, *Senior Member, IEEE*

***Abstract*— Charge pumping (CP) has proved itself to be one of the most utilitarian methods to quantify defects in MOS devices. In the presence of low-to-moderate gate leakage, CP quantification is most often implemented via a series of measurements at multiple frequencies. However, this approach is ill-equipped to handle excessive leakage currents common in advanced technologies. In this paper, we transform multifrequency CP from a quasi-dc measurement into a true ac measurement. This ac detection scheme, called frequency-modulated CP, is far better equipped to deal with high levels of leakage currents and thereby extends the usefulness of CP to current and future device technologies where excessive leakage is the norm. Additionally, we show that multifrequency CP has a long overlooked error that becomes significant in high-leakage situations. We discuss the origins of this error in detail and outline mitigation methodologies. Finally, we explore timing and voltage limitations of waveform generators and how these experimental boundary conditions impact on both frequency-dependent and FMCP.**

***Index Terms*— Charge pumping (CP), defects, leakage current.**

I. Introduction

CHARGE pumping has historically been an extremely powerful and easily implemented tool for MOSFET defect monitoring [1]–[5]. However, the successful collection and interpretation of CP data has become increasingly more challenging. The main driver of this difficulty is the ever increasing CP current (I_{CP})-to-gate leakage current (I_{leak}) ratio. Simply put, device area scaling minimizes I_{CP} while dielectric thickness scaling maximizes I_{leak}. This presents a CP precision issue that requires the measurement of a very small signal (I_{CP}) riding on top of an extremely large background (I_{leak}). In this difficult experimental scenario, CP is quickly falling out of favor as a go-to defect feedback tool.

Manuscript received April 2, 2014; revised January 8, 2015; accepted January 20, 2015. The review of this paper was arranged by Editor E. Rosenbaum.

J. T. Ryan, J. P. Campbell, and K. P. Cheung are with the Semiconductor and Dimensional Metrology Division, National Institute of Standards and Technology, Gaithersburg, MD 20899 USA (e-mail: jason.ryan@nist.gov; jason.campbell@nist.gov; kin.cheung@nist.gov).

J. Zou and R. Huang are with the Department of Microelectronics, Peking University, Beijing 100871, China (e-mail: zoujibin@gmail.com; ruhuang@pku.edu.cn).

R. Southwick III is with IBM Research, Albany, NY 12233 USA (e-mail: rgsouthwick@gmail.com).

A. S. Oates is with Taiwan Semiconductor Manufacturing Corporation, Hsinchu 30844, Taiwan (e-mail: aoates@tsmc.com).

Color versions of one or more of the figures in this paper are available online at http://ieeexplore.ieee.org.

Digital Object Identifier 10.1109/TED.2015.2395956

Recently, we have demonstrated a CP methodology called frequency-modulated CP (FMCP) that robustly treats the I_{leak} issue and extends the usefulness of CP [6]–[8]. With the ability to measure CP in such high-leakage situations, we discovered a long-overlooked CP error, a frequency-dependent I_{leak} component. In this paper, we extend our earlier FMCP work to investigate the frequency dependence of this component; the origins are described and validated through a series of simple calculations. Methodologies to mitigate this error, experimental proofs of concept, and the implications of experimental limitations are also discussed.

II. Conventional Charge Pumping

In the simplest mode of conventional CP, a square wave voltage pulse (50% duty cycle) is applied to the gate such that the MOSFET is cyclically pulsed between strong accumulation and strong inversion at some frequency, f (typically in the kHz-to-MHz range) [1]–[3]. In doing so, interface defects are alternately populated with electrons or holes. The source, drain, and substrate electrodes are grounded while the (quasi-dc) CP recombination current (I_{CP}) is measured at the substrate. In the absence of bulk defects [9]–[11], gate leakage [5], and the well-known geometric effect [1], [2], [12], I_{CP} scales linearly with the CP gate pulse frequency such that

$$I_{\mathrm{CP}} = q A f D_{\mathrm{it}} \Delta E \tag{1}$$

where q is the electronic charge, A is the device area, D_{it} is the energetic and areal interface state density ($\mathrm{cm}^{-2}\ \mathrm{eV}^{-1}$), and ΔE is the CP recombination energy window [3]. For the case of pulsing between strong inversion and strong accumulation, the ΔE window is roughly the entire band gap. Emission loss near the band edges narrows the ΔE window [1], [2], but is reduced by minimizing the rise (t_r) and fall (t_f) times of the gate waveform. In a modern standard implementation, I_{CP} is measured as a function of CP frequency (f), the slope of which is proportional to the number of defects probed [1], [2] providing a quick and easy measure of D_{it}.

In the presence of gate leakage, the substrate current (I_{sub}) is the sum of I_{CP} and a leakage component that flows through the substrate (I_{leak}). Built into the standard approach is the assumption that I_{leak} is independent of f. The most common leakage corrections usually involve either: (1) a multifrequency measurement in which the extrapolated value of I_{sub} at $f = 0$ Hz is subtracted from the data as a dc offset [5], [13] or (2) subtraction of a low-frequency

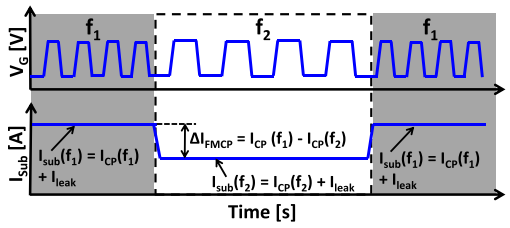

Fig. 1. Schematic of FMCP showing the modulated gate waveform (top) and the resulting ac-coupled substrate current (bottom). By employing an ac-coupled detection scheme, the difference between I_{CP} at two different frequencies (ΔI_{FMCP}) can be measured with a high degree of precision.

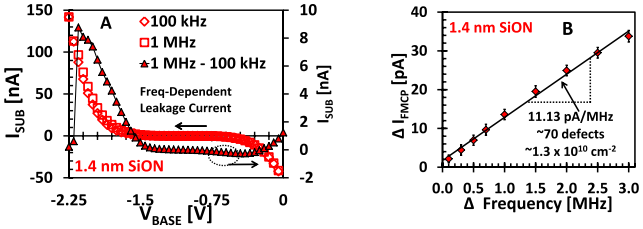

Fig. 2. (A) Conventional Elliot curve and high/low frequency subtraction fails due to the enormous leakage background. (B) Despite this, FMCP is able to resolve a linear frequency-dependent CP slope on the device in (A).

Elliot curve from its high-frequency counterpart [5]. These approaches are intuitive and straightforward. Unfortunately, two serious problems arise when I_{leak} becomes much larger than the I_{CP}.

First, I_{leak} can be so dominant that the method of extracting the small I_{CP} signal from the much larger I_{sub} becomes highly unreliable. Precision errors occur when taking the difference of two large numbers (I_{sub} at two frequencies). Since single-digit populations of defects matter in highly scaled devices [14], even modest precision uncertainty introduces significant analysis error. One possible solution is to increase the magnitude of I_{CP} relative to I_{leak}. Equation (1) points to the intuitive approach of increasing f to increase I_{CP} relative to the frequency-independent background [15]–[19]. However, square waveform shapes become difficult to maintain at higher frequencies. Thus, many GHz CP efforts instead utilize sine waves to sweep the gate [17]–[19]. Unfortunately, sine waves also present inherent problems. As the frequency increases, the time for trap-filling during each CP half cycle decreases and incomplete trap filling [3], [13] becomes a concern. The result is a smaller fraction of defects within ΔE are able to participate. This leads to ambiguous decreases in charge per cycle and hence analysis errors [13]. Sine waves present a situation where the gate voltage is always changing; since the device never reaches a (quasi) equilibrium state, emission loss leads to further analysis errors.

The second serious problem arising from large leakage I_{CP} measurements lies in the assumption of frequency-independent I_{leak}. While intuitive and physically correct, in actuality this assumption is flawed. As will be discussed later in detail, a careful examination of the CP gate pulse reveals a small frequency-dependent leakage effect mainly caused by additional time spent in rise/fall transition times at higher frequencies. When leakage is large, this effect becomes noticeable and introduces errors in the measure of pure CP.

III. Frequency-Modulated Charge Pumping

In the simplest sense, FMCP is similar to the above discussed high/low frequency subtraction approach. The key advancement is a more intelligent detection scheme that enhances the immunity to high levels of leakage. This is accomplished by *modulating* the gate pulse between two (or more) frequencies. A schematic of the modulated gate waveform and the corresponding I_{sub} is shown in Fig. 1.

The gate waveform is modulated between two frequencies, f_1 and f_2. Modulation depth is defined as $(f_1 - f_2)/2$ and is symmetric about some center frequency. While the gate is at f_1, a dc current is observed, $I_{sub}(f_1) = I_{CP}(f_1) + I_{leak}$. When switched to f_2, the dc current now becomes $I_{sub}(f_2) = I_{CP}(f_2) + I_{leak}$. Here, $f_2 < f_1$ and thus $I_{sub}(f_2) < I_{sub}(f_1)$. Switching back to f_1, the process repeats and the net observable result is an I_{sub} that oscillates between the two values.

Very similar to the high/low frequency subtraction method and assuming frequency-independent I_{leak}, if we subtract $I_{sub}(f_1)$ and $I_{sub}(f_2)$, I_{leak} cancels out and we are left with a CP signal equal to $I_{CP}(f_1 - f_2)$. The key advancement in FMCP is the detection scheme utilized to measure $I_{CP}(f_1 - f_2)$. In the conventional approach, separate measurements are made at each frequency and the data are subtracted offline leading to the aforementioned precision errors. In FMCP, I_{CP} $(f_1 - f_2)$, defined here as ΔI_{FMCP}, is an ac signal. Hence, employing an ac-coupled detection scheme nearly eliminates the I_{leak} background and the precision uncertainties associated with conventional CP approaches. As discussed elsewhere [6], [7], ac coupled ΔI_{FMCP} lends itself perfectly to lock-in amplifier detection by phase locking to the modulation frequency. Alternatively, the ac-coupled signal can be directly observed using an oscilloscope, which is useful for visualization of the ac signal and confirmation of signal integrity. This mode also supports two or more frequency modulation schemes [6].

To showcase the robustness of FMCP, we demonstrate the technique on a production quality 1.4-nm SiON 10 μm $\times$ 0.055 μm nMOSFET which exhibits relatively high levels of gate leakage. Fig. 2(A) shows an attempt at conventional Elliot curve measurements on the high-leakage device for two frequencies. The voltage amplitude is 2 V and $t_r/t_f = 5$ ns. Clearly, the measured I_{sub} is completely dominated by leakage and any CP signal is completely unresolvable. Fig. 2(A) also shows an attempted high/low frequency subtraction (1 MHz–100 kHz) result [5]. Unfortunately, the data still contain no useful information as the levels of leakage are too great to permit a precise and accurate extraction of I_{CP}.

A simple calculation highlights the difficulty encountered in Fig. 2(A). If we assume, for example, that the 1.4-nm SiON device has $D_{it} = 1.5 \times 10^{10}$ cm^{-2}, the expected I_{CP} at 1 MHz, from (1), is roughly 10 pA. This value is orders of magnitude smaller than the tens of nA leakage background (not shown). From a precision viewpoint, it is

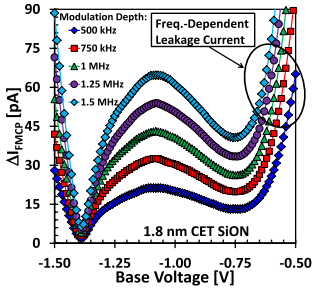

Fig. 3. FMCP detected Elliot curves for the 1.8-nm CET SiON device. At first glance, FMCP enables the observation of very clear Elliot curve peaks. However, a closer examination reveals a seemingly frequency-dependent component in regions that do not support CP recombination.

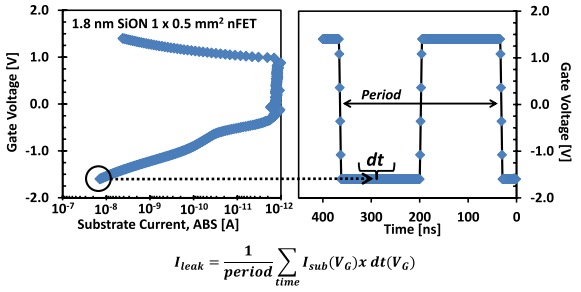

Fig. 4. Schematic of a typical square-wave gate pulse (right) compared with asymmetric dc-measured leakage current (absolute value) (left). Leakage is most dominant during high/low voltages and less important during transitions.

immediately clear that measuring this signal is experimentally very difficult.

Despite the overwhelmingly large leakage and the failed conventional attempts, FMCP is capable of providing useful information. Fig. 2(B) shows lock-in detected frequency-dependent FMCP data taken on the same device in Fig. 2(A). In this case, the Δ frequency axis refers to the modulation depth. A linear $\Delta I_{\mathrm{FMCP}} - \Delta f$ relationship exists (well within one standard deviation), equating to about 70 defects in the device. This information was obtained despite the suffocating levels of leakage which rendered the conventional approaches useless. This demonstration illustrates the capabilities of FMCP and the precision boost gained from ac detection. Furthermore, this clearly demonstrates why FMCP is a much needed and powerful technique for advanced devices where gate leakage stymies defect related development feedback and reliability monitoring [6].

IV. Assumption of Frequency-Independent Leakage

As noted, conventional CP and FMCP embodiments rely on the intuitive assumption that I_{leak} is independent of frequency. In its truest meaning, there is no reason to believe otherwise. However, when the gate waveform is nonideal (nonzero t_r and t_f), the gate leakage effectively becomes frequency dependent. For illustrative purposes, Fig. 3 shows a series of Elliot curves at various frequencies obtained via lock-in detected FMCP on a 10 μm $\times$ 0.035 μm 1.8-nm capacitance equivalent thickness (CET) SiON nMOSFET (from [7]) that displays extraordinarily high gate leakage (not shown). At first glance, clear Elliot curve signals are present. However, a more careful examination reveals a frequency-dependent component when the base voltage is raised toward inversion (highlighted region) where no CP should occur (recombination not supported). Similarly, a careful examination of the conventional high/low frequency subtraction shown in Fig. 2(A) (highlighted region) also reveals a frequency-dependent component in a region not supported by CP. If there is a frequency-dependent current in regions where I_{CP} should be zero, it is reasonable to expect that such a component contributes to the measured CP signal as well.

The frequency-dependent leakage is the result of nonzero t_r and t_f of the gate waveform. The largest leakage occurs during the high- and low-voltage portions of the gate pulse as

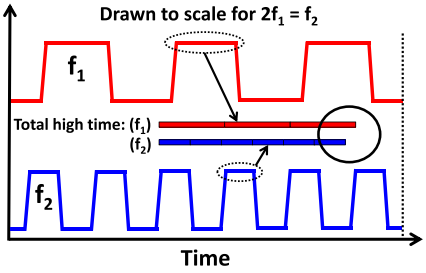

Fig. 5. Drawn-to-scale illustration of two waveforms where f_2 is double the frequency of f_1 with fixed rise/fall times. Since f_2 goes through twice the number of transitions per unit time, less total time is spent at high (and low) voltage. This is manifested as a frequency-dependent leakage component.

illustrated in Fig. 4. Since the leakage is asymmetric, the result is a nonzero leakage observable in CP. However, if the time spent at high and low voltage is frequency independent, then leakage is also frequency independent. Due to finite t_r and t_f and that higher frequencies equate to more rise/fall edges per unit time, the time spent at the high and low voltage becomes frequency dependent, leading to frequency-dependent leakage.

The effect is schematically drawn to scale in Fig. 5 by comparing two waveforms (f_1 and f_2) of equal t_r/t_f with f_2 double the frequency of f_1. As shown, the higher frequency waveform (f_2) goes through twice the number of transitions per unit time. Since transitions are finite, less total time is spent at high (and low) voltages at the higher frequency.

Note that this is true of *any* multifrequency CP measurement including conventional high/low frequency subtraction [5, Fig. 2(A)], linear extrapolation to 0 Hz CP, and FMCP (Fig. 3). This is an error that has long been overlooked and clearly invalidates the assumption of frequency-independent leakage in CP measurements.

Simple calculations utilizing the *measured* leakage data of Fig. 4 further illustrate this idea. Pure I_{CP} is calculated from (1), emission loss is not treated, and we assume full probing of the bandgap (maximum ΔE). Defect density is taken as 10^{10} cm^{-2} and I_{CP} is plotted versus frequency in Fig. 6(A) (top).

Calculated I_{leak} versus frequency is also shown in Fig. 6(A) (bottom) for various rise and fall times. I_{leak} is calculated by summing all the charges that leak through the gate to the substrate during a quasi-dc gate voltage sweep (Fig. 4) and then integrating this charge over one gate waveform period (equation shown in Fig. 4). Clearly, the leakage

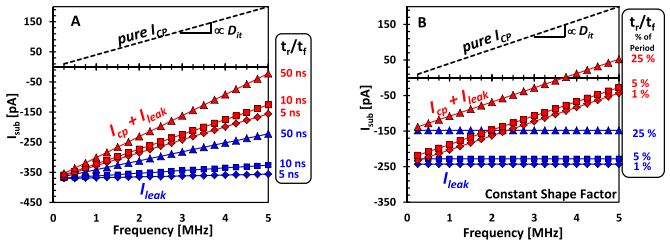

Fig. 6. (A) Calculation of I_{leak} reveals a frequency dependence that clearly impacts on the I_{CP} response resulting in a slope change and erroneous defect density extraction. (B) Implementation of the constant shape factor restriction eliminates the frequency-dependent leakage and allows accurate and self-consistent defect density extractions.

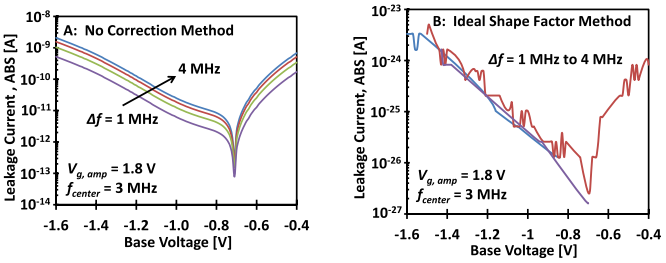

Fig. 7. (A) When no timing restrictions are enforced, conventional methods display large leakage with clear frequency dependence. (B) Enforcement of the constant shape factor restriction results in negligible leakage current. The data appear incomplete due to null residual leakage current values.

current in Fig. 6(A) displays the troublesome linear frequency dependence and increases with increasing rise/fall times. It is this nature of the frequency-dependent leakage that makes it indistinguishable from pure I_{CP}. Since the only experimental observable is the net I_{sub}, the summation of the frequency-dependent I_{leak} and I_{CP} [Fig. 6(A), bottom] results in an erroneous I_{CP} versus frequency slope and consequent erroneous defect density extraction.

V. Constant Shape Factor Method

Since frequency-dependent I_{leak} lies in the unintentional frequency-dependent distribution of high/low times per pulse period, elimination of this error can be accomplished through careful timing control of the gate waveform.

A constant shape factor restriction, described in greater detail in [7], forces the low time/rise time and high time/fall time ratios of the waveform to remain equal and constant for all utilized frequencies. At higher frequencies, the high/low time is shorter and the constant shape factor method requires a correspondingly shorter rise/fall time. These restrictions result in a constant fractional time spent on rising/falling edges, independent of frequency.

Implementation of a constant shape factor in our simple calculations [Fig. 6(A)] results in frequency-*independent* I_{leak}, which is insensitive to rise/fall times. This is shown in Fig. 6(B) for several different cases where the rise/fall times occupy several different percentages of the pulse period. More importantly, the constant shape factor criteria results in an accurate I_{CP} versus frequency slope; allowing accurate and consistent defect density extractions.

The constant shape factor concept can also be demonstrated in a calculation more relevant to FMCP (along with almost all other multifrequency CP methods). Using similar approaches to that of Fig. 6 to calculate I_{leak} using the measured data, Fig. 7 shows simulated I_{leak} as a function of base voltage for various modulation depths. The data shown are obtained by calculating I_{leak} for two frequencies and then subtracting. Note that, in these Elliot curve like figures, CP is not included; only residual leakage after subtraction is. When plotted in this fashion, the voltage and frequency dependence can be easily observed.

Rather large leakage, displaying clear frequency dependence, is observed in Fig. 7(A) where no timing restrictions are implemented. However, the enforcement of an ideal constant shape factor [Fig. 7(B)] eliminates the effect to negligible current levels.

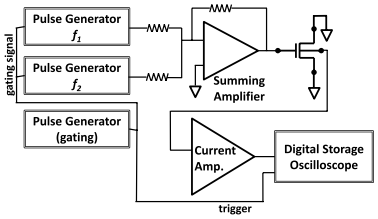

Fig. 8. Schematic of one possible implementation of constant shape factor FMCP. Two standalone pulse generators provide f_1 and f_2 while being gated by a third pulse generator at the modulation frequency. f_1 and f_2 are fed through a simple summing amplifier which drives the gate of the device. ΔI_{FMCP} is detected via a current amplifier and digital storage oscilloscope (lock-in detection can also be used).

While excessive alteration of rise/fall times can introduce undesirable emission loss [2], [3] effects, the typical variations need to enforce a constant shape factor (a few ns) has a relatively minor effect which is outweighed by the benefit of a frequency-independent I_{leak}. We note that a sine waveform naturally dictates constant shape factor. However, the emission loss/incomplete trap filling issues synonymous with sine wave CP discussed above are so troubling that the constant shape factor attribute is significantly overshadowed.

VI. Constant Shape Factor Proof of Concept

Ideal implementation of constant shape factor criteria requires extremely tight gate waveform timing (sub-ns range) and voltage control (mV) of the various CP frequencies. While high-end waveform generators are capable of this, most economical versions are lacking. The practical consequences of nonideal timing and voltage control are discussed in later sections. For experimental proof of concept, however, we use two standalone gated pulse generators driving a summing circuit (Fig. 8). The generators provide the two FMCP frequencies (f_1 and f_2) and are gated (at the modulation frequency) such that the summing amplifier output (fed to the device gate) is a modulated f_1/f_2 waveform. While not ideal, this simple arrangement allows individual control of each frequency in an economical and convenient manner.

Using such an arrangement, constant shape factor FMCP was experimentally demonstrated for a 1.8-nm CET SiON 1 μm $\times$ 0.06 μm nMOSFET. Shown in Fig. 9(A) is a series of constant amplitude (1.8 V) swept base voltage Elliot curves at various modulation depths. Fig. 9(B) shows the

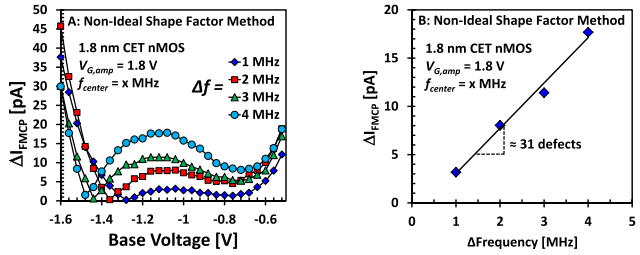

Fig. 9. (A) Utilizing a nonideal arrangement, constant shape factor FMCP data indicate a suppression of the frequency-dependent I_{leak}. (B) Extraction of ΔI_{FMCP} versus frequency from (A) indicates that this technique is well suited to extend CP to highly scaled and highly leaky technologies.

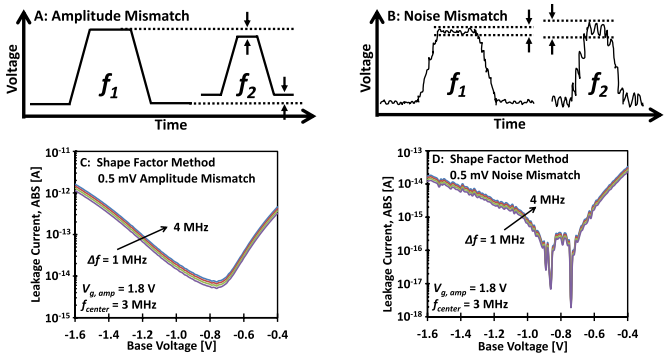

Fig. 10. (A) Voltage amplitude mismatch. (B) Noise mismatch. (C) Relatively small amplitude mismatch and (D) noise mismatch in the constant shape factor method produces a frequency-dependent residual leakage.

frequency-dependent CP extracted from the Elliot curve peaks (around -1.1 V) in (A). Note that some frequency dependence still exists in regions that do not support CP. However, compared with similar results of Fig. 3 without shape factor control, the frequency-dependent I_{leak} component is greatly suppressed.

The incomplete elimination of frequency-dependent leakage is due to timing and voltage resolutions of our source generators. This experiment thus serves only as a proof of concept. This result also demonstrates the utility of constant shape factor FMCP to probe highly scaled device geometries with exceedingly small numbers of defects.

As discussed, frequency-dependent I_{leak} is the result of the time spent at high/low waveform portions. It then follows that altering the duty cycle is another method to directly control high/low time distributions. Since I_{leak} is gate voltage dependent, implementation of an ideal duty cycle criteria requires a voltage-dependent duty cycle variation (more duty cycle variation is required where there are larger leakage currents). This voltage-dependent duty cycle variation results in significant experimental difficulty. However, simulations similar to those shown in Fig. 7 indicate that the duty cycle method also suppresses the frequency-dependent leakage (not shown).

VII. Waveform Nonidealities—Voltage Uncertainty

We now discuss in greater detail the implications of nonideal waveform characteristics on the CP signal. Fig. 10(A) and (B) shows two common types of voltage nonidealities, amplitude mismatch and noise mismatch, respectively. Amplitude (noise) mismatch occurs when the amplitude (noise) of f_1 does not perfectly match the amplitude (noise) of f_2.

First we examine amplitude mismatch in a constant shape factor scenario, using the same procedures used to obtain the Elliot curve-like residual leakage of Fig. 7. Various amplitude mismatches were purposely included such that the high voltage and low voltage of f_1 and f_2 are both slightly mismatched (0.5 mV shown). The noise amplitudes and all other relevant characteristics of the two frequencies are identical. Therefore, a 0 mV mismatch case is a perfectly ideal implementation and produces the same negligible residual leakage, as shown in Fig. 7. When a slight amplitude mismatch is introduced, shown in Fig. 10(C), the effect is a significant increase in residual frequency-dependent leakage. It is important to point out that the value used (0.5 mV) is a very minor mismatch; with a nominal waveform amplitude of 1.8 V, an 8-bit (12-bit) waveform generator has a minimum voltage resolution of about 7 mV (0.45 mV). Clearly, the constant shape factor criterion will push the specifications of waveform generators to their limits.

Next we examine the noise mismatch nonideality in a constant shape factor scenario. Again, we use the same procedures as before to obtain the residual leakage. In this case, a 0.5 mV pk–pk amplitude noise mismatch was used [Fig. 10(D)]. All other characteristics are identical. We first note that the background residual leakage is much lower when compared with Fig. 10(C) and is accentuated with larger noise mismatch (not shown). The curves also display the undesirable frequency dependence. While noise mismatch produces a relatively small effect compared with the amplitude mismatch, noise should still be taken into consideration. For example, in highly scaled devices, the number of defects present can be small such that the expected I_{CP} is only hundreds of fA, even with MHz FMCP frequencies. While small, the effects shown in Fig. 10(D) can have a meaningful negative impact on analysis.

VIII. Waveform Nonidealities—Timing Uncertainty

The second type of waveform nonideality is timing uncertainty. Fig. 11(A) and (B) schematically shows two types of timing uncertainty, horizontal skew and slope skew, respectively. Horizontal skew and slope skew are due to a clock timing uncertainty which results in an artificial variation in high/low times. The result is a shape factor that is not quite constant; it is immediately clear that these timing errors will introduce frequency-dependent I_{leak}.

First we examine horizontal skew for the constant shape factor method. The calculations involve the same procedures utilized for the two types of voltage mismatch. In this case, a horizontal skew is purposely included at various levels in such a manner that the high voltage time is increased while the low voltage time is decreased, both by 0.5 ns (all other being equal) as shown in Fig. 11(C). The opposite scenario, where the high time is decreased while the low time is increased,

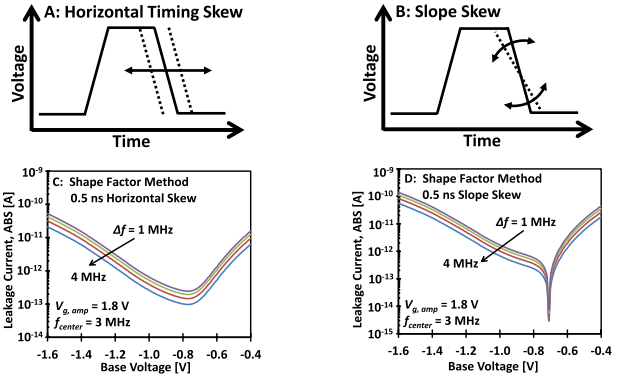

Fig. 11. (A) Horizontal skew. (B) Slope skew. Both have the effect of artificially changing the shape factor of the waveforms. (C) Relatively small horizontal skew and (D) slope skew in the constant shape factor method produces a frequency-dependent residual leakage.

produces nearly identical results (not shown). Compared with voltage uncertainties (Fig. 10), horizontal skew is clearly a much more serious problem (note the vertical scales).

Next, we explore the effect of slope skew. Here, we purposely introduce a slope skew in such a manner that the rise/fall times are both decreased by 0.5 ns. The opposite scenario in which the rise/fall times are increased produces similar results (not shown). Fig. 11(D) shows the slope skew effect and it is clear that a large residual leakage background exists as well as the undesirable frequency dependence.

Similar to the voltage nonidealities, horizontal skew and slope skew are entirely limited by the instrument performance and are present to varying degrees in every waveform generator. While arbitrary waveform generators with very tight timing resolution (100-ps range) are commercially available, most common and more economical instruments have minimum timing specifications in the range of the values we have chosen (about 1 ns). Thus, similar to the voltage uncertainties, the level of shape factor control will be limited by instrumentation and must be considered.

IX. Waveform Nonidealities—Combined Uncertainty

No waveform generator is perfect; each and every instrument contains amplitude mismatch, noise mismatch, horizontal skew, and slope skew to varying degrees. The number of possible combinations of uncertainties and values chosen can become quite large, and thus, we simply show the result of all uncertainties combined. In Fig. 12, we purposely introduce a 2.0-mV voltage amplitude mismatch, a 0.5-mV noise mismatch, a 2.0-ns horizontal skew, and a 1.0-ns slope skew.

The result is a large residual leakage component displaying frequency dependence. These combined uncertainties affect the resulting I_{leak} so much that the use of correction methodologies produces no improvement. Obviously, there are instrument packages that are capable of much better results, as demonstrated here (Fig. 9) where significant improvement was achieved. However, commercially available arbitrary waveform generators typically used for communications

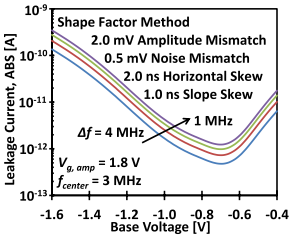

Fig. 12. Combined uncertainty of all four nonidealities displaying large residual leakage with strong frequency dependence.

research do have promising specifications which will likely enable further mitigation of the frequency-dependent I_{leak} present in most CP measurements.

X. Conclusion

We have demonstrated a CP methodology called FMCP that provides vast improvement in precision and is highly resistant to gate leakage currents. In high-leakage devices, where conventional approaches simply do not work, FMCP easily provides the sought-after information. In addition, we discuss a long-overlooked error in any multifrequency CP measurement manifested as a frequency-dependent leakage component. Methods to eliminate this effect as well as other instrumentation considerations are described. FMCP provides a clear path toward defect measurements and defect energy profiling in highly scaled advanced technologies where gate leakage becomes problematic and hinders development progress.

References

[1] J. S. Brugler and P. G. A. Jespers, "Charge pumping in MOS devices," *IEEE Trans. Electron Devices*, vol. 16, no. 3, pp. 297–302, Mar. 1969.

[2] G. Groeseneken, H. E. Maes, N. Beltran, and R. F. De Keersmaecker, "A reliable approach to charge-pumping measurements in MOS transistors," *IEEE Trans. Electron Devices*, vol. 31, no. 1, pp. 42–53, Jan. 1984.

[3] G. Van den Bosch, G. V. Groeseneken, P. Heremans, and H. E. Maes, "Spectroscopic charge pumping: A new procedure for measuring interface trap distributions on MOS transistors," *IEEE Trans. Electron Devices*, vol. 38, no. 8, pp. 1820–1831, Aug. 1991.

[4] A. B. M. Elliot, "The use of charge pumping currents to measure surface state densities in MOS transistors," *Solid-State Electron.*, vol. 19, no. 3, pp. 241–247, 1976.

[5] P. Masson, J. Autran, and J. Brini, "On the tunneling component of charge pumping current in ultrathin gate oxide MOSFETs," *IEEE Electron Device Lett.*, vol. 20, no. 2, pp. 92–94, Feb. 1999.

[6] J. T. Ryan, J. P. Campbell, K. P. Cheung, J. S. Suehle, R. G. Southwick, and A. S. Oates, "Reliability monitoring for highly leaky devices," in *Proc. IEEE Int. Rel. Phys. Symp.*, Apr. 2013, pp. 2D.5.1–2D.5.4.

[7] J. T. Ryan *et al.*, "Constant shape factor frequency modulated charge pumping (FMCP)," in *Proc. IEEE Int. Integr. Rel. Workshop Final Rep.*, Oct. 2013, pp. 21–25.

[8] J. T. Ryan, R. G. Southwick, J. P. Campbell, K. P. Cheung, A. S. Oates, and J. S. Suehle, "Frequency-modulated charge pumping: Defect measurements with high gate leakage," *IEEE Electron Device Lett.*, to be published.

[9] D. Heh *et al.*, "Spatial distributions of trapping centers in HfO_2/SiO_2 gate stack," *IEEE Trans. Electron Devices*, vol. 54, no. 6, pp. 1338–1345, Jun. 2007.

[10] J. T. Ryan, R. G. Southwick, J. P. Campbell, K. P. Cheung, and J. S. Suehle, "On the contribution of bulk defects on charge pumping current," *IEEE Trans. Electron Devices*, vol. 59, no. 11, pp. 2943–2949, Nov. 2012.

[11] M. Masuduzzaman, A. E. Islam, and M. A. Alam, "Exploring the capability of multifrequency charge pumping in resolving location and energy levels of traps within dielectric," *IEEE Trans. Electron Devices*, vol. 55, no. 12, pp. 3421–3451, Dec. 2008.

[12] G. Van den Bosch, G. Groeseneken, and H. E. Maes, "On the geometric component of charge-pumping current in MOSFETs," *IEEE Electron Device Lett.*, vol. 14, no. 3, pp. 107–109, Mar. 1993.

[13] J. T. Ryan *et al.*, "Spectroscopic charge pumping investigation of the amphoteric nature of Si/SiO_2 interface states," *Appl. Phys. Lett.*, vol. 98, no. 23, pp. 233502-1–233502-3, Jun. 2011.

[14] A. Asenov, R. Balasubramaniam, A. R. Brown, and J. H. Davies, "RTS amplitudes in decananometer MOSFETs: 3-D simulation study," *IEEE Trans. Electron Devices*, vol. 50, no. 3, pp. 839–845, Mar. 2003.

[15] R. Fernandez *et al.*, "AC NBTI studied in the 1 Hz–2 GHz range on dedicated on-chip CMOS circuits," in *Proc. IEEE Int. Electron Devices Meeting*, Dec. 2006, pp. 1–4.

[16] M. Cho *et al.*, "Interface trap characterization of a 5.8-AA EOT p-MOSFET using high-frequency on-chip ring oscillator charge pumping technique," *IEEE Trans. Electron Devices*, vol. 58, no. 10, pp. 3342–3349, Oct. 2011.

[17] G. T. Sasse and J. Schmitz, "Charge pumping at radio frequencies: Methodology, trap response and application," in *Proc. 44th Annu. IEEE Int. Rel. Phys. Symp.*, Mar. 2006, pp. 627–628.

[18] G. T. Sasse and J. Schmitz, "Application and evaluation of the RF charge-pumping technique," *IEEE Trans. Electron Devices*, vol. 55, no. 3, pp. 881–889, Mar. 2008.

[19] Y. Wang and K. P. Cheung, "Carrier capture at the SiO_2–Si interface: A physical model," *Appl. Phys. Lett.*, vol. 91, no. 11, pp. 113509-1–113509-3, Sep. 2007.

Authors' photographs and biographies not available at the time of publication.